

IMAGE MISSION ATTITUDE SUPPORT EXPERIENCES[†]

N. Ottenstein, M. Challa, A. Home*

Computer Sciences Corporation, 7700 Hubble Drive, Lanham-Seabrook, Maryland USA 20706

R. Harman, R. Burley

NASA Goddard Space Flight Center, Greenbelt, MD 20771

ABSTRACT

The spin-stabilized Imager for Magnetopause to Aurora Global Exploration (IMAGE) is the National Aeronautics and Space Administration's (NASA's) first Medium-class Explorer Mission (MIDEX). IMAGE was launched into a highly elliptical polar orbit on March 25, 2000 from Vandenberg Air Force Base, California, aboard a Boeing Delta II 7326 launch vehicle. This paper presents some of the observations of the flight dynamics analysts during the launch and in-orbit checkout period through May 18, 2000.

Three new algorithms - one algebraic and two differential correction - for computing the parameters of the coning motion of a spacecraft are described and evaluated using in-flight data from the autonomous star tracker (AST) on IMAGE. Other attitude aspects highlighted include: support for active damping consequent upon the failure of the passive nutation damper, performance evaluation of the AST, evaluation of the Sun sensor and magnetometer using AST data, and magnetometer calibration.

INTRODUCTION

This paper describes some of the major events during IMAGE in-orbit checkout (IOC) and also presents new algorithms that were developed for the use of attitude processing during this period. Attitude support was predominantly via an enhanced version of the Multimission Spin Axis Stabilized Spacecraft Attitude Determination System (MSASS), which is the controlled software used in the Flight Dynamics Facility at NASA GSFC. Note that, only highlights during IOC support are presented here; more detailed analyses and system descriptions are given in Refs. 1 and 2.

The octagon-shaped IMAGE spacecraft is 2.25 m in diameter by 1.52 m height and weighs 494 kg, including its instrument payload. There are four thin radioplasma imager (RPI) radial antennas, positioned 90 deg apart, which define the spacecraft X-Y plane while the two RPI axial antennas define the Z-axis. When fully extended, the axial antennas measure 20 m tip-to-tip, and the radial antennas 500 m.

[†] This paper was supported by the National Aeronautics and Space Administration (NASA) Goddard Space Flight Center (GSFC), Greenbelt, Maryland, under Contract: GS-35F-4381G, Task Order: S-43411-G. IMAGE mission support was performed under NASA GSFC Contract: GS-35F-4381G, Task Order: S-36490-G.

* E-mail: nottenst@cscmail.csc.com, Phone: (301) 794-2437

IMAGE was placed into an orbit that had an apogee altitude of about 45885 km (~ 7 Earth-radii), an inclination of 90.008 deg, and an eccentricity of 0.752624. It is spin-stabilized about its Z-axis, with closed-loop spin-rate control. Following separation from the launch vehicle the attitude determination and control subsystem was required to align the spin axis parallel to the nominal attitude within 1° of negative orbit normal and with a spin rate between 0.5 and 20 revolutions per min (rpm). Once attitude acquisition was accomplished and the antenna deployments were completed, the spin rate is to be maintained at 0.5 ± 0.01 rpm. During nominal mission (commencing approximately 40 days after separation) the attitude knowledge is to be within 0.1° for both spin phase angle and spin axis RA and DEC while maintaining the spin rate at 0.5 ± 0.01 rpm.

The IMAGE attitude hardware consists of: one Lockheed Martin ATC AST-201R autonomous star tracker (AST), one Adcole 44690 Sun sensor assembly (SSA), one MEDA model TAM-2A three-axis magnetometer (TAM), an Ithaco model 750UPR magnetic torque rod (MTR), and a nutation damper (ND). These are described in detail in Ref. 3.

EVENT TIME LINE

There were several major events during IOC. This time period consisted of several stages of interest.

The first stage was from launch on March 25, 2000 until April 2, 2000. This stage include the following events:

- The satellite was first checked out and it was discovered that the nutation was not damping.
- An initial procedure to decrease the spin rate of the satellite increased the nutation.
- After considerable analysis it was decided that the onboard passive nutation damper was malfunctioning, and that active nutation damping must be used to reduce the nutation.
- Several spin-downs were performed before active nutation damping could be attempted, even though these did increase the nutation.
- The first attempt to reduce the nutation on April 1, 2000 actually increased the nutation as it was done 180 deg out of phase. More details on the failure of the nutation damper and the actions to deal with it are discussed in the Ref. 4.

Figure 1 shows the Sun angle for the first full day of operation (March 26, 2000). The Sun angle is the angle between the spin axis vector (the Z-axis) and the Sun. The Sun sensor boresight is elevated 1.922 deg above the spin plane and the plots do not compensate for this bias. There is one point every spin period. The spin period at this time is about 19.4 seconds. The figure shows no noticeable damping of the nutation. It also appears that there was a slight gravity gradient effect at the first perigee and possibly a thermal effect from the eclipse, which adjusted the attitude slightly. The slope in the Sun angle for the two orbits shown in the figure is clearly different. Figure 2 shows the effects of two spin down procedures on the Sun angle. The spin period was changed from ~20.3 seconds to ~22 seconds and then to ~26.5 seconds. As seen, the nutation was slightly increased each time and the attitude was changed as is shown by the change in the mean Sun angle.

The second stage of interest was from April 3, 2000 through April 10, 2000. During this time the nutation was actively damped by use of the torquers. During the last few days of this period the spin rate was reduced to 0.75 rpm. Once the satellite was at this rate the AST was turned on and began tracking stars. Figure 3 shows the nutation in the Sun angle damped to less than 0.001 deg on April 9, 2000. It shows a clear gravity gradient effect in the Sun angle near perigee, as indicated by the change of slope in the Sun angle.

The third stage of interest was the reorientation of the attitude towards negative orbit normal. This was from April 10, 2000 through April 14, 2000. Figure 4 shows the AST quaternions during the first attitude maneuver towards negative orbit normal. The data gap towards the lower right of the figure is when the AST lost track due to Earth occultation. More discussion of the AST is presented later in this paper. The attitude circles have a radius that is of the nutation angle at the time.

The fourth stage was the spin-up in order to deploy the radial booms. This was from April 15, 2000 through April 19, 2000. The AST lost track shortly into the first spin-up at a point above 1.123 rpm as was expected from the AST specifications

The final stage involved the RPI antenna deployments. The radial booms were deployed from April 20, 2000 through May 13, 2000. The Z-axis booms were deployed on May 14, 2000. The AST was turned on again and began tracking towards the end of the first deployment on April 20.

Figures 5 and 6 show the first 125 m of deployment of the radial booms, preceded by another segment of active nutation damping. A gravity gradient effect coming out of perigee is also seen. Figure 6 shows in more detail the effects of the deployment, which induced new frequencies in the attitude behavior.

IOC ended on May 18, 2000.

STAR TRACKER PERFORMANCE

The AST was able to calculate attitudes that could be verified with the Sun angle data.

During the spin-up after attitude acquisition the AST lost track due to rising spin rate at about GMT 415.0126. The spacecraft was in eclipse with the spin rates before and after eclipse being 1.123 and 1.434 rpm respectively.

Figure 7 compares predicted (using AST quaternions) and observed Sun angles for a full day. The known Sun angle bias is taken into account in this figure. The straight line is the predicted Sun angles calculated from the AST quaternion generated attitude. The mean difference is 0.098 deg with a standard deviation of 0.012 deg. At these Sun angles the specified error in the Sun sensor is 0.25 deg so the AST result is well within that.

As discussed previously, the AST did lose track during the first attitude maneuver, and during the early mission timeframe it lost track a few more times near perigee. The first occurrence was thought to have been caused by Earth occultation, but the subsequent dropouts did not have the Earth interfering with the AST. It is now believed that the dropouts near perigee were due to radiation, which interfered with the charge-coupled device readings. By default, the AST drops into a standby mode after three consecutive acquisition failures. The flight operations team (FOT) changed it from 3 to 256 attempts and this resulted in satisfactory "on-times" of the AST.

Figure 8 shows the AST losing track during a perigee and then regaining it later. The perigee was at Greenwich Mean Time (GMT) 0546. There was also an eclipse during GMT 0543-0551. It shows the RA versus time. Note that as the AST lost track the quaternions registered a constant default value, and resumed the oscillations (due to coning) when tracking was regained. At this time the angle between the spin axis and the Sun vector was about 144 deg, which is about only 26 deg away from the AST boresight. Later, after the IOC period the star tracker lost track at a closer Sun angle. This was believed to be due to contamination from stray sunlight. The problem disappeared when the Sun was further away from the AST.

MSASS SUN-ONLY SOLUTIONS

The differential correction (DC) algorithm (i. e., batch least-squares estimator) in MSASS solves for a constant spin-axis attitude from SSA data. These solutions used data over the course of 6 to 12 hours. However the attitude varied significantly during early mission due to nutation and smaller effects such as gravity-gradient torques. Thus the DC Sun-only solutions (when the algorithm converged) during early mission have larger errors, which are estimated to be about half the nutation angle.

The initial MSASS attitude solution was (203, 53) deg where, as in the rest of this paper, the first number is the right ascension (RA) and the second number is the declination (DEC) in the geocentric inertial frame (GCI). This was about 6.8 deg away from the expected a priori attitude of (213.7, 50.9) deg. As noted in the event timeline (and seen in Figures 2 and 5), the spin and attitude changed because of the active nutation damping. Accurate and reliable attitudes were available only after AST became operational on 4/10/00, the first AST attitude being (201.16, 61.77) deg.

The best procedure for obtaining Sun-only attitude would be by taking constant attitude data from successive apogees. Unfortunately, due to active damping occurring at perigees, there was rarely a case when the attitude was not changed between apogees. Thus data were taken only during a single orbit. A key assumption in getting Sun-only attitude solutions is that the attitude is a constant. Once the AST was turned on, it was noticed that there was a considerable drift in the attitude over an orbit. A drift of 0.2 deg in DEC over the course of an orbit was often seen. This changing DEC also contributed to the inability of obtaining a reliable Sun-only solution if the RA and DEC were allowed to vary from their a priori values.

MSASS PREDICTION AND ONBOARD PROCESSOR SUPPORT (POPS) UTILITY

The multi-mission nature of MSASS was helpful during the IOC when POPS (which is normally used to predict Earth cuts by horizon sensors) was used in three originally unanticipated situations. In one early situation it was used to verify antenna contact angle during a period when contact with the spacecraft was lost. Later, by using the AST parameters (instead of those of a horizon sensor), the utility was used to check for Earth-occultation of the AST during the first attitude maneuver. Finally, POPS was also useful in generating Sun angle predictions for various attitudes. This was used to validate the Sun sensor telemetry as well as to predict times when the Sun would be outside the Sun sensor field of view.

MSASS CONING ANGLE (CA) UTILITY

Theory

The CA utility computes the parameters of uniform coning by a spacecraft, and was included in MSASS as part of IMAGE attitude support (Ref. 5). Given a history of the spacecraft attitude, $\{\hat{S}(\alpha_i, \delta_i) | i = 1, 2, \dots, N\}$, coning about an unknown cone axis, $\hat{S}_c(\alpha_c, \delta_c)$, this utility computes (α_c, δ_c) and the cone half-angle, θ . Here α and δ generally denote RA and DEC respectively. A sketch of the scenario is given in Figure 9.

The principal algorithm in the CA utility is the Batch-Cone algorithm, which is a DC algorithm that estimates the above cone parameters. To overcome possible convergence issues, two new "circle" algorithms - Triplet and Batch-Circle - were also implemented for computing the a priori Batch-Cone state vector. These circle algorithms are an approximation, for they compute the center and radius of a circle in RA-DEC space given the coordinates of circumference points, which are the tips of \hat{S} in Figure 9. Such a circle is not an unrealistic approximation during the IMAGE nominal mission mode when the cone axis is expected to be the GCI y-axis, although it could be drastically incorrect for other mission geometries such as when coning is about the GCI z-axis. (See the CA evaluation below for a scenario where the circle approximation does not hold.) Of the two circle algorithms, Batch-Circle is a differential corrector whereas Triplet is a pure-algebraic algorithm without any convergence issues. The Triplet algorithm can be particularly useful when the measurements are available over only a small arc in RA-DEC space, for the algorithm is very general and will yield the center even if only 3 points are available. By default, CA uses all three algorithms in sequence: Triplet, whose results are input to Batch-Circle, whose results are input to Batch-Cone.

These three algorithms are described next. Note that, although we assume here that GCI is the input/output reference frame, the choice of frame is not essential to the computations - the components of the cone axis are in the same frame as the input vectors.

The Batch-Cone Algorithm

The state vector is the 3x1 vector, \vec{X} , defined via:

$$\vec{X} = [\alpha_c \ \delta_c \ \theta]^T, \quad (1)$$

where the superscript "T" denotes matrix transpose. As usual \vec{X}^0 denotes the a priori state while \vec{X} denotes the current one, and S0 denotes the 3x3 diagonal matrix of user-specified weights associated with \vec{X}^0 . Noting that

$\hat{S}_c = [\cos \delta_c \cos \alpha_c \quad \cos \delta_c \sin \alpha_c \quad \sin \delta_c]^T$, with a similar expression for the i -th attitude vector, $\hat{S}_i(\alpha_i, \delta_i)$, the angle θ_i between \hat{S}_i and \hat{S}_c is given by

$$\cos \theta_i = \cos \delta_i \cos \alpha_i \cos \delta_c \cos \alpha_c + \cos \delta_i \sin \alpha_i \cos \delta_c \sin \alpha_c + \sin \delta_i \sin \delta_c. \quad (2)$$

We seek an estimator which would make all the θ_i identical in the ideal noise-free scenario. Accordingly, the vector of residuals, $\bar{\rho} = [\rho_1 \rho_2 \dots \rho_N]^T$ is constructed from:

$$\rho_i = \theta_i - \theta, \quad i = 1, 2, \dots, N. \quad (3)$$

The theoretical development is similar to that in Ref. 6, except that, for simplicity, all the residuals were given the equal weight of $1/(\Delta\theta)^2$, where $\Delta\theta$ is user-specified. The loss function, J , is defined via:

$J = \frac{1}{2} \frac{\bar{\rho}^T \bar{\rho}}{(\Delta\theta)^2} + \frac{1}{2} [\bar{X} - \bar{X}^0]^T S^0 [\bar{X} - \bar{X}^0]$. Minimizing J with respect to the components of \bar{X} yields the following matrix equation:

$$G^T \bar{\rho} = S^0 (\bar{X} - \bar{X}^0) (\Delta\theta)^2, \quad (4)$$

where the elements of the $N \times 3$ matrix G are given by:

$$G_{ik} = -\partial \rho_i / \partial X_k, \quad i = 1, 2, \dots, N, \quad k = 1, 2, 3, \quad (5)$$

Let $G^0 \equiv G(\bar{X}^0)$, i. e.,

$$G^0 \equiv \begin{bmatrix} -\frac{\partial \theta_i}{\partial \alpha_c} \Big|_{\bar{X}_0} & -\frac{\partial \theta_i}{\partial \delta_c} \Big|_{\bar{X}_0} & 1 \\ \dots & \dots & \dots \\ -\frac{\partial \theta_N}{\partial \alpha_c} \Big|_{\bar{X}_0} & -\frac{\partial \theta_N}{\partial \delta_c} \Big|_{\bar{X}_0} & 1 \end{bmatrix}, \quad (6)$$

which can be readily computed using Eq. (2). We can compute ρ_i using ρ_i^0 and G^0 via:

$$\bar{\rho} \approx \bar{\rho}^0 - G^0 (\bar{X} - \bar{X}^0). \quad (7)$$

Using Eq. (7) and approximating G by G^0 in Eq. (4) yields the leading order formula for the state innovation:

$$\bar{X} - \bar{X}^0 = \left[G^{0T} G^0 + S^0 (\Delta\theta)^2 \right]^{-1} G^{0T} \bar{\rho}^0. \quad (8)$$

If $\bar{X} - \bar{X}^0$ is greater than a user-specified tolerance, the algorithm is repeated after setting $\bar{X}^0 = \bar{X}$.

The Batch-Circle Algorithm

It is assumed here that the attitude history $\{\alpha_i, \delta_i\}$ traces an arc of a circle whose center is at (α_c, δ_c) and whose radius is r . The 3×1 state vector is defined as: $\bar{X} = [\alpha_c \ \delta_c \ r]^T$. We now seek an estimator that would make all the radii identical in the ideal noise-free scenario. Accordingly, the residual vector is constructed from: $\rho_i = r_i - r$, $i = 1, 2, \dots, N$, where

$$r_i = \sqrt{(\alpha_i - \alpha_c)^2 + (\delta_i - \delta_c)^2}. \quad (9)$$

The development is similar to that of the Batch-algorithm. As before, all the residuals have the equal weight of $1/(\Delta r)^2$, with G^0 now given by:

$$G^0 \equiv \begin{bmatrix} \frac{(\alpha_1 - \alpha_c^0)}{r_1^0} & \frac{(\delta_1 - \delta_c^0)}{r_1^0} & 1 \\ \dots & \dots & \dots \\ \frac{(\alpha_N - \alpha_c^0)}{r_N^0} & \frac{(\delta_N - \delta_c^0)}{r_N^0} & 1 \end{bmatrix}, \quad (10)$$

and the state innovation given by: $\bar{X} - \bar{X}^0 = \left[G^{0T} G^0 + S^0 (\Delta r)^2 \right]^{-1} G^{0T} \bar{\rho}^0$.

Denoting the final converged values of the state by the superscript "f", $\{\theta_i^f\}$ are computed using (α_c^f, δ_c^f) in Eq.

(2). The cone parameters are then obtained using: $\hat{S}_c^f = \begin{bmatrix} \cos \delta_c^f \cos \alpha_c^f & \cos \delta_c^f \sin \alpha_c^f & \sin \delta_c^f \end{bmatrix}^T$

and $\theta^f = \sum_{i=1}^n \theta_i^f / n$.

The Triplet Algorithm

This algorithm computes the center, (α_c, δ_c) , and radius, r , of the circle given three points (α_1, δ_1) , (α_2, δ_2) , and (α_3, δ_3) on the circumference of a circle. Let r_{ic} be the distance between the i -th circumference point and the center, i. e., the i -th radius. Demanding $r_{1c} = r_{2c}$ and $r_{2c} = r_{3c}$ yields respectively:

$$2\alpha_c(\alpha_1 - \alpha_2) + 2\delta_c(\delta_1 - \delta_2) = (\alpha_1^2 - \alpha_2^2) + (\delta_1^2 - \delta_2^2), \quad (11)$$

$$2\alpha_c(\alpha_2 - \alpha_3) + 2\delta_c(\delta_2 - \delta_3) = (\alpha_2^2 - \alpha_3^2) + (\delta_2^2 - \delta_3^2). \quad (12)$$

Multiplying Eq. (11) by $(\delta_2 - \delta_3)$, Eq. (12) by $(\delta_1 - \delta_2)$, subtracting, and re-arranging the terms yields:

$$\alpha_c = \frac{1}{2} \left[\frac{(\alpha_1^2 + \delta_1^2)(\delta_2 - \delta_3) + (\alpha_2^2 + \delta_2^2)(\delta_3 - \delta_1) + (\alpha_3^2 + \delta_3^2)(\delta_1 - \delta_2)}{\alpha_1(\delta_2 - \delta_3) + \alpha_2(\delta_3 - \delta_1) + \alpha_3(\delta_1 - \delta_2)} \right], \quad (13)$$

$$\delta_c = -\frac{1}{2} \left[\frac{(\alpha_1^2 + \delta_1^2)(\alpha_2 - \alpha_3) + (\alpha_2^2 + \delta_2^2)(\alpha_3 - \alpha_1) + (\alpha_3^2 + \delta_3^2)(\alpha_1 - \alpha_2)}{\alpha_1(\delta_2 - \delta_3) + \alpha_2(\delta_3 - \delta_1) + \alpha_3(\delta_1 - \delta_2)} \right]. \quad (14)$$

To overcome noise, the averages (α_c^f, δ_c^f) over several triplets are computed. The cone parameters \hat{S}_c^f and θ^f are then computed as in the Batch-Circle algorithm. A set of radii is computed using Eq. (9) and the average value is input to the Batch-Circle algorithm. The principal advantage of the Triplet algorithm is that it yields results even when only 3 points are available, although one must ensure that these data are well separated when processing noisy data.

Performance of the Coning Angle Utility

In practice, the utility was used as follows. An a priori attitude solution was obtained by using the triplet algorithm, which was fed to the Batch-Cone algorithm. This solution then was fed into the Batch-Cone algorithm for the final solution. Figure 10 is an output of the Coning Angle Utility using 6 min (720 points), i.e., 3 spin periods, of IMAGE in-flight data. Here circles represent the attitude history and an asterisk at the center of the circle represents the estimated cone axis. The Batch-Cone algorithm yielded (283.226, -0.24619) deg for (α_c, δ_c) and 0.196 deg for the cone angle. The Batch-Circle and Batch-Cone algorithms converged here in 2 and 1 iterations respectively, and yielded very small residuals - less than 0.01 deg - thus indicating that the estimation was accurate. (Note that the circle approximation is not a drastic one here; in fact, since the "circle" is complete, a simple averaging of the (RA, DEC) data yielded reasonable values of (283.211, -0.246) deg for (α_c, δ_c) .) When only 30 sec of the same data were input, the Batch-Cone algorithm yielded (283.202, -0.249) deg for (α_c, δ_c) and 0.170 deg for the cone angle, results not far from the definitive ones using 6 min of data. In general, data spanning 1/2 spin period yield results which are essentially no different from those obtained using 3 spin periods of data.

A dramatic example of the usefulness of the Batch-Cone algorithm is presented in Figure 11 which presents results using noise-free simulated data of coning close to the GCI z-axis. One cone period (240 points) of spin axis data were generated with truth model parameters of: $(\alpha_c, \delta_c) = (75, 80)$ deg, $\theta_c = 15$ deg. These are shown in Figure 11 as circles (points 1 - 144) as well as dashes (points 145 - 240). Note that the (RA, DEC) plot of the attitude history is not even a closed curve, let alone a circle. Thus intuition as well as Batch-Circle and Triplet algorithms are of no use here in determining the characteristics of the motion. The Batch-Cone algorithm was directly run, using a priori values of: $(\alpha_c^0, \delta_c^0) = (60, 64)$ deg, $\theta_c^0 = 12$ deg, and only 60% of the attitude history (points 1-144). The algorithm converged in 10 iterations to within 0.1 deg of all the parameters (see the legend in the figure). It should be emphasized that the Batch-Cone algorithm does not always perform as well; in fact, both batch algorithms usually do not converge if a priori errors are over 20%.

TAM AND MTR PERFORMANCE

The TAM biases were estimated by simply examining the field at apogee which is at 7 Earth radii. This yielded biases of (-12.05, +4.42, -17.25) mG in BCS. The MTR coupling coefficients were computed by Lockheed Martin Missiles and Space Division (LMMS) personnel separately via in-flight tests at apogee on 3/26/00, and were found to be changed only slightly from their pre-launch values. Numerous instances were seen, however, of differences between the TAM and MTR timetags. An example of this is shown in Figure 12, where TAM and MTR data are compared near an apogee on 3/26/00. The top plot of this figure shows that there is significant MTR current until 9318 sec. The middle plot, however, shows that the TAM measurements dropped significantly at about 9307 sec. (The bottom plot shows that the magnitudes are near zero during 9300 sec - 9307 sec after accounting for the MTR currents.)

Additional evidence of TAM timetag issues can be seen in Figure 13 where we see large differences between the predicted and measured Sun-magnetic field angle (which is attitude-independent) on 3/26/00. Note that timetag errors of a few seconds are sufficient to generate large angular errors since IMAGE was spinning at 3 rpm at that time. Reliable three-axis attitude and rates could not therefore be computed using SSA and TAM data; some interesting simulations of effects of timetag errors are given in Ref. 1.

MAGNETIC FIELD MODELS AND PREDICTIONS

A consequence of the failure of the nutation damper was that nutation damping had to be accomplished actively using the MTR to generate the appropriate magnetic control torques near the perigees in early April 2000. This required unplanned attitude support involving the generation of 3-hour spans of predicted magnetic fields (via non-MSASS utilities at NASA-GSFC called the Flight Dynamics Toolbox) at over 30 perigees. The input here consisted of an estimated spin axis attitude from the MSASS Sun-only solutions, and ephemeris data. The field predictions were generated during early April. The accuracy of the predictions could occasionally be evaluated only after the AST became operational after 4/10/00. Nevertheless, it was possible, sometimes, to evaluate the TAM after the AST was powered-on on 4/10/00. It was seen that the measured fields at apogee were within 5 mG of the predictions (which were used to estimate the extent of active damping). A particularly revealing example is provided in Figure 14, where the axis-wise predictions (using AST attitudes) are compared with measurements at an apogee of 4/26/00. The bias calibration yields good agreement even at 7 Earth radii. (Note that the plots do not include periods of MTR activity at which times large TAM residuals were again seen.)

SUMMARY

There were several lessons learned during the support.

Pre-launch simulations were useless from an attitude support point of view due to the lack of sensor data with any fidelity. Various telemetry problems were discovered early in the mission. Practically immediately it was discovered that the bits of the sun sensor telemetry were reversed from the specifications. This was quickly corrected in the software. Similarly, there were the previously mentioned timetag problems with the TAM/MTR. End-to-end tests are needed resolve data issues while the spacecraft is still on the ground.

Despite the above, many of the difficulties were quickly overcome due to constant communications between the attitude analysts and developers, the FOT, and LMMS personnel during early operations. The close contacts also facilitated quick responses to the nutation damper anomaly by, for example: (1) creating several different versions of the MSASS telemetry processor function to process different data formats, (2) predicting antenna contacts, (3) predicting perigee magnetic fields, and (4) keeping personnel schedules flexible.

The new MSASS Coning Angle utility worked as intended and was useful during and after the IOC period. The new algorithms introduced for estimating the cone parameters are very general and should be useful in future missions.

REFERENCES

1. M. Challa, N. Ottenstein, A. Home, and M. Marchowsky, *Imager for Magnetopause to Aurora Global Exploration (IMAGE) Attitude Support Post-Launch Report*, prepared by Computer Sciences Corporation (CSC) for NASA GSFC, Greenbelt, MD, June 30, 2000
2. A. Home, M. Marchowsky, N. Ottenstein, and M. Challa, *Imager for Magnetopause to Aurora Global Exploration (IMAGE) Multimission Spin Axis Stabilized Spacecraft (MSASS) Attitude Determination System - User's Guide Version 2.5*, prepared by CSC for NASA GSFC, Greenbelt, MD, June 30, 2000
3. LMMS/P458668A, *IMAGE Spacecraft/Observatory - Spacecraft Description and Operator's Manual CDRL A028 (FINAL)*, LMMS, Sunnyvale, CA 94088-3504, January 5, 1999
4. C. Hubert and D. Swanson, "Surface Tension Lockup in the IMAGE Nutation Damper - Anomaly and Recovery." *2001 Flight Mechanics Symposium, NASA/CP—2001-209986*, 2001. (Paper 39 of this compilation.)
5. M. Challa and A. Home, *Coning Angle Utility - Functional Specifications*, prepared by CSC for NASA GSFC, Greenbelt, MD, January 14, 2000
6. J. S. Wertz (Editor), *Spacecraft Attitude Determination and Control*, D. Reidel Publishing Co., Dordrecht, Holland, 1978, pp. 449–451

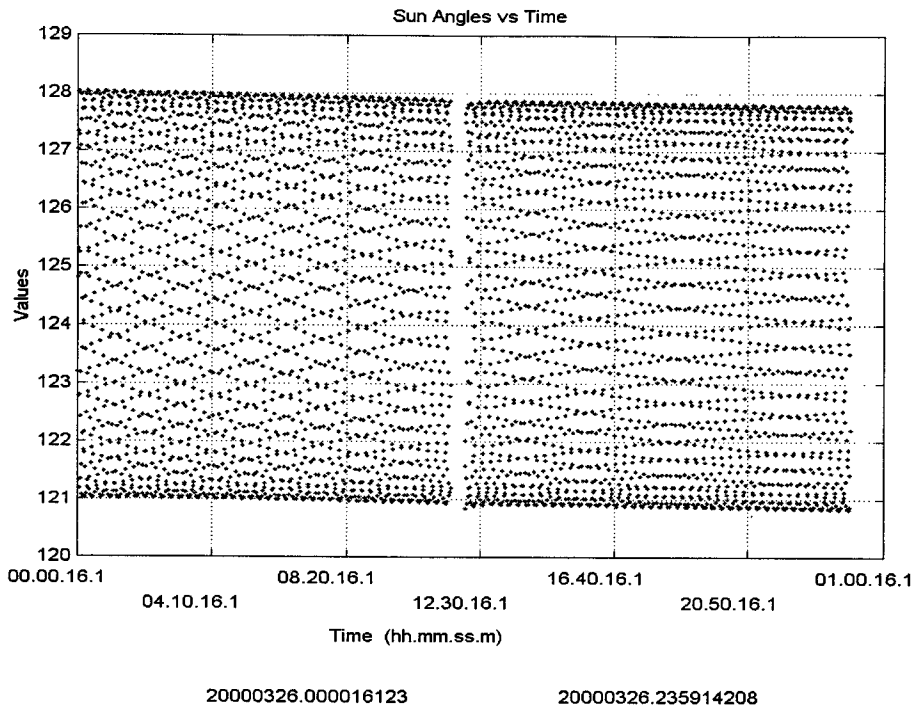


Figure 1 Sun Angles (Deg) During the First Full Day of Operations

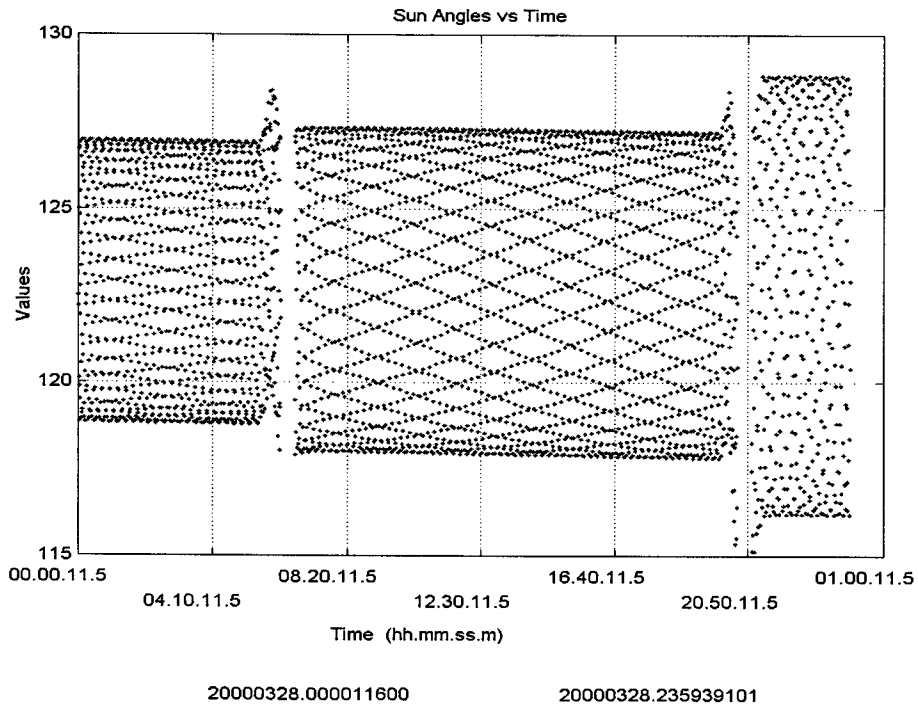


Figure 2 Sun Angles (Deg) During the 2nd and 3rd Spin-Down Procedures

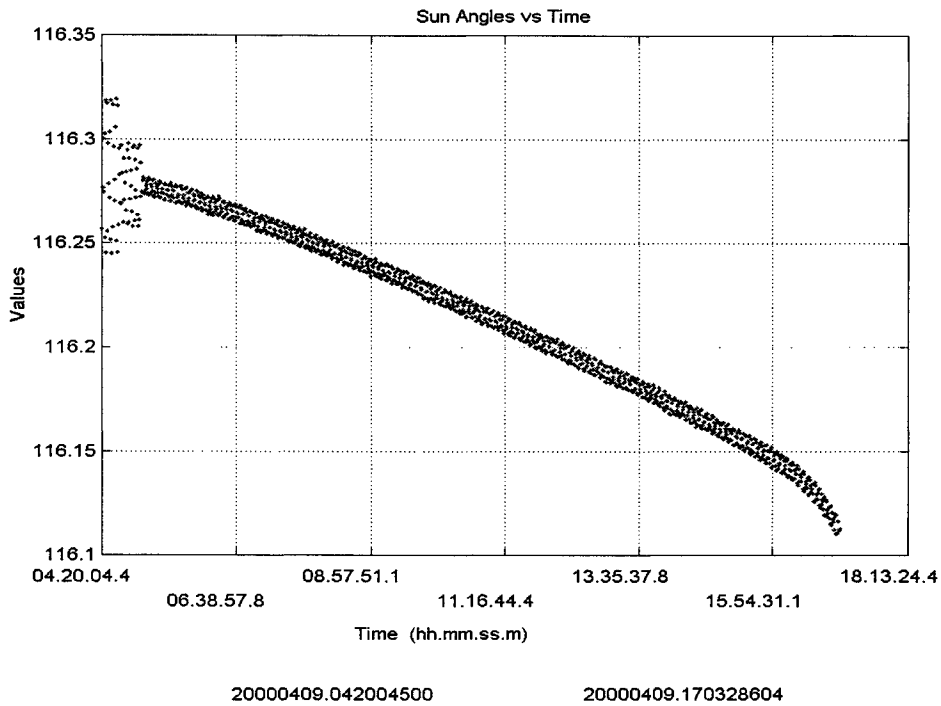


Figure 3 Sun Angle Data (Deg) Showing Gravity-Gradient Effects

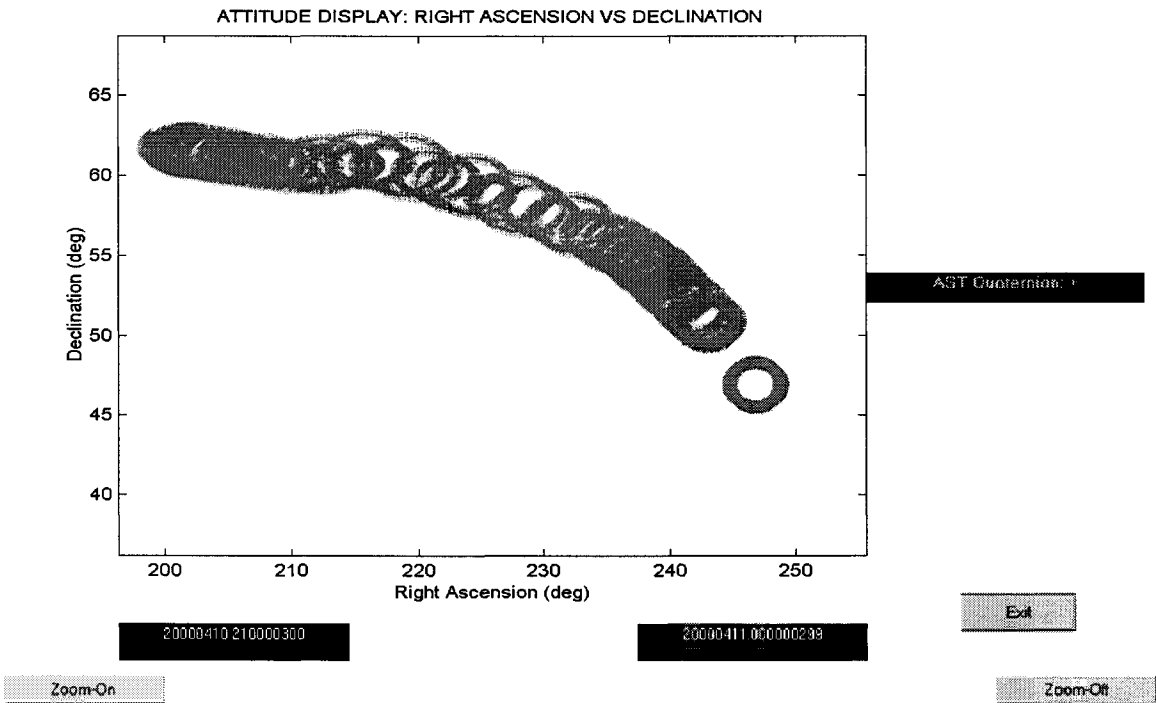


Figure 4 AST Attitude Data During the First Reorientation

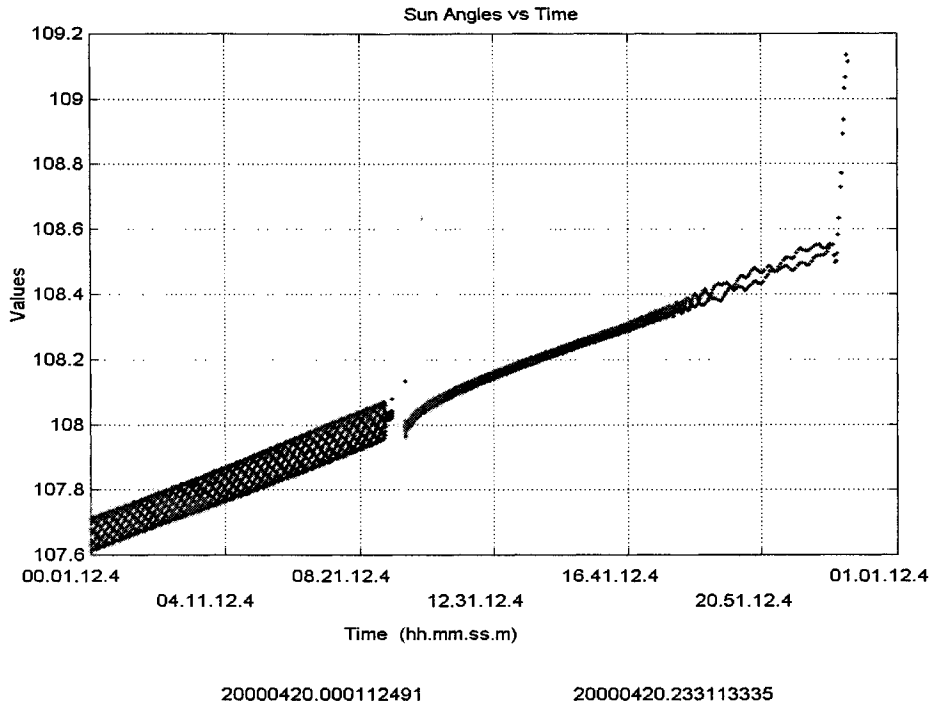


Figure 5 Sun Angle Data (Deg) During Radial Boom Deployment to 125 m

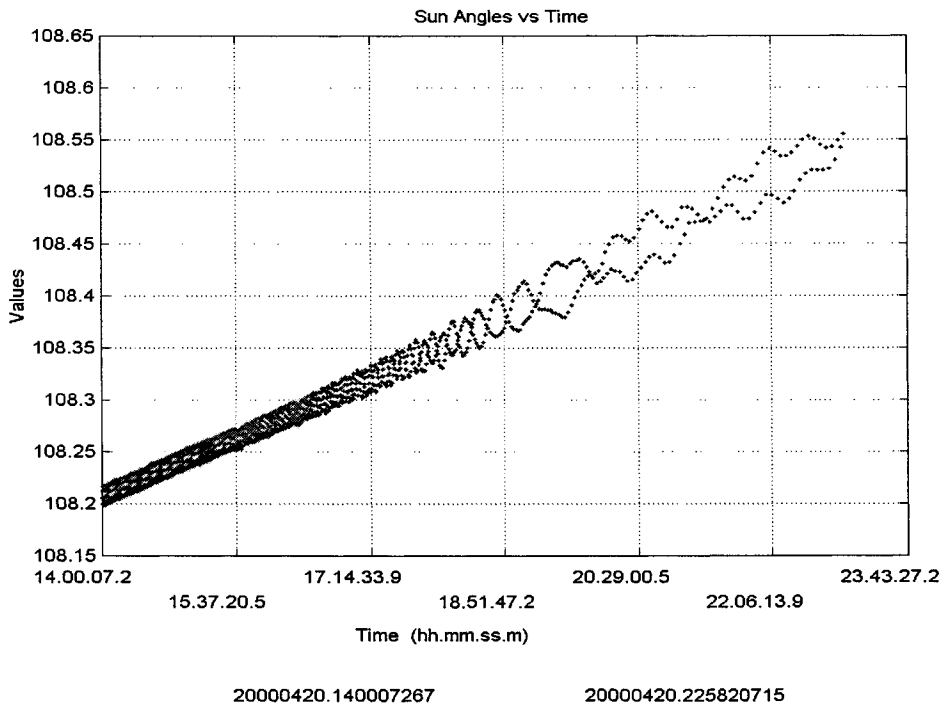


Figure 6 A Close-Up View of Figure 5 - Sun Angles (Deg)

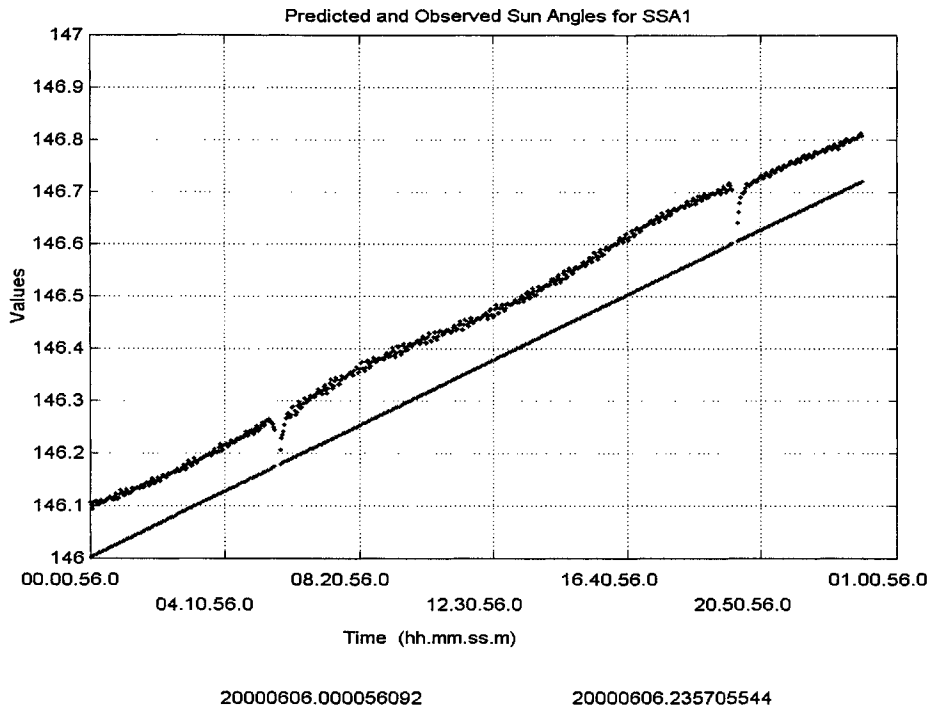


Figure 7 Comparison of AST-Predicted and Observed Sun Angles (Deg)

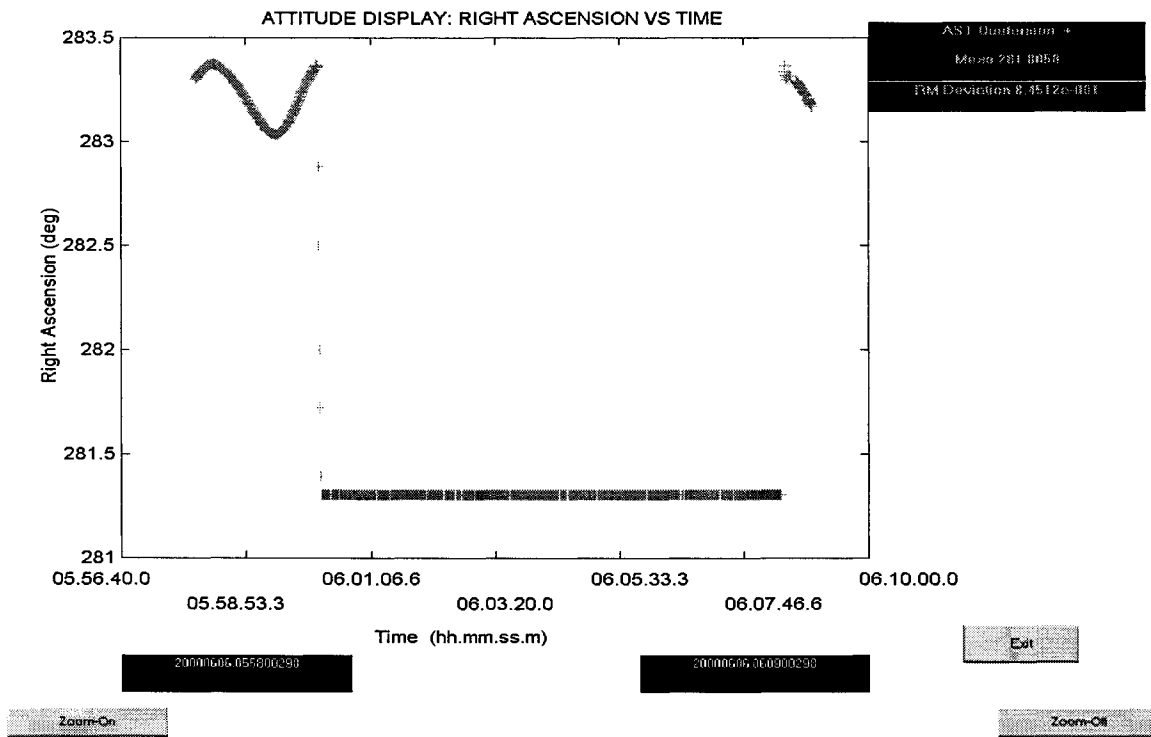


Figure 8 AST RA History Showing AST Dropout

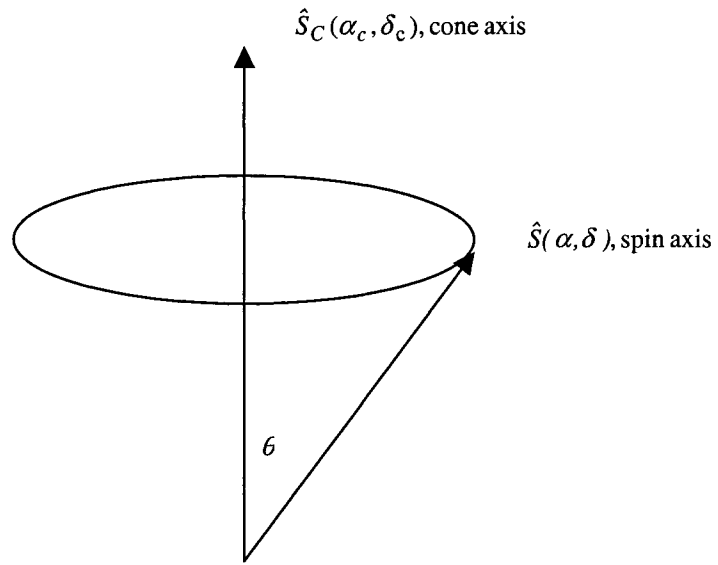


Figure 9 Schematic of Spacecraft Coning

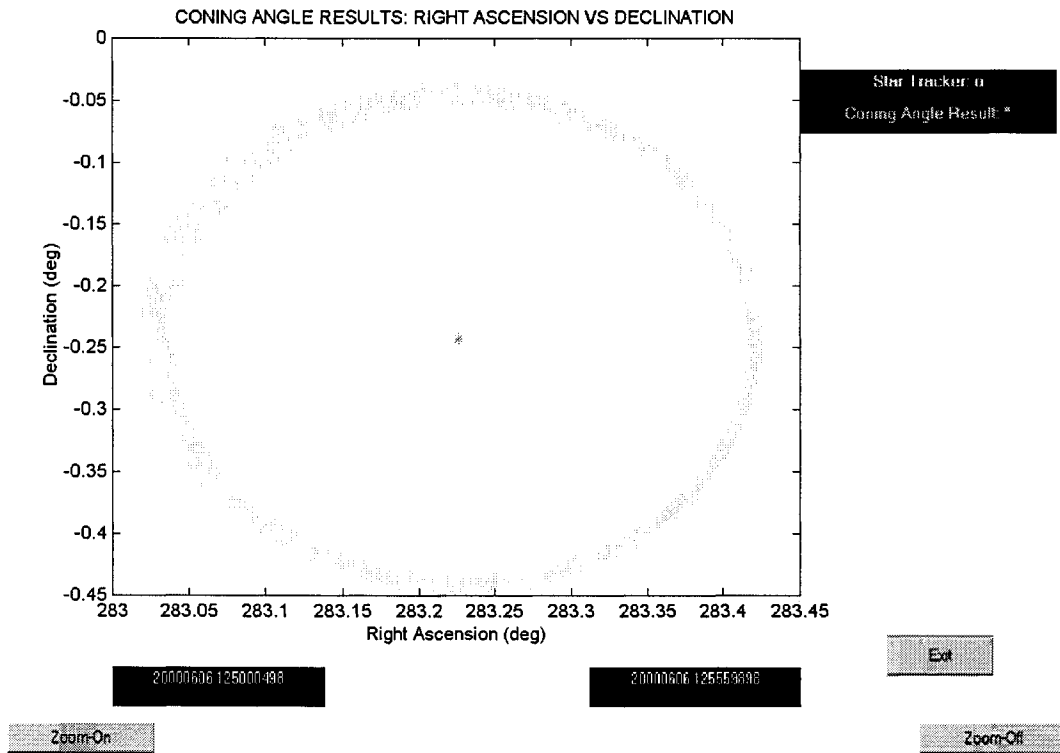


Figure 10 DEC vs. RA plot of 3 Spin Periods of IMAGE Data with Coning Angle Solution (Center)

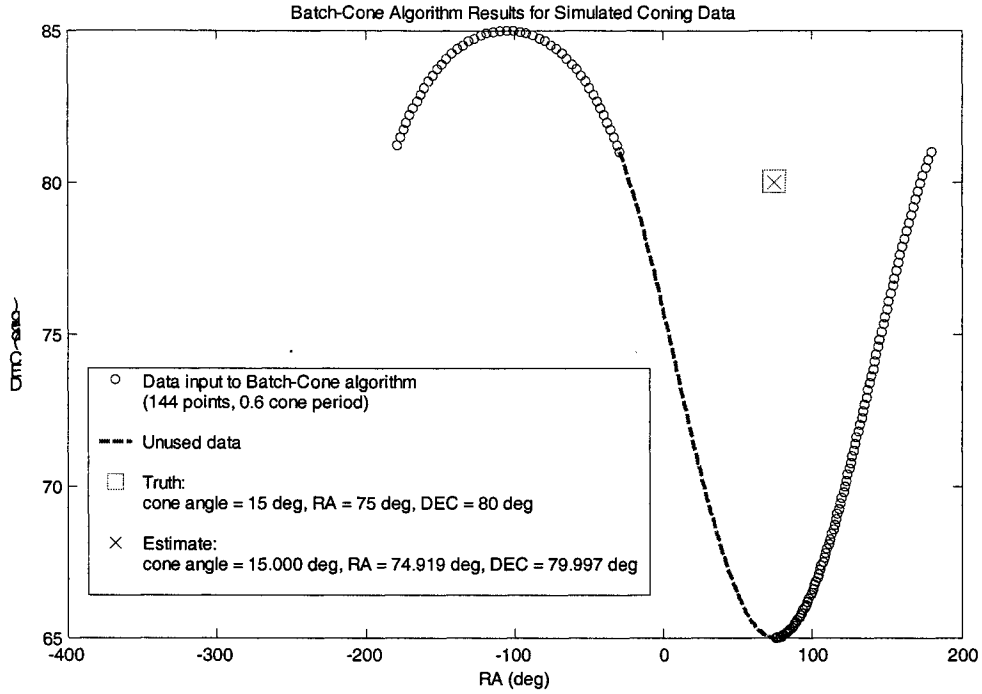


Figure 11 Batch-Cone Algorithm Results for Simulated (non-IMAGE) Coning Data

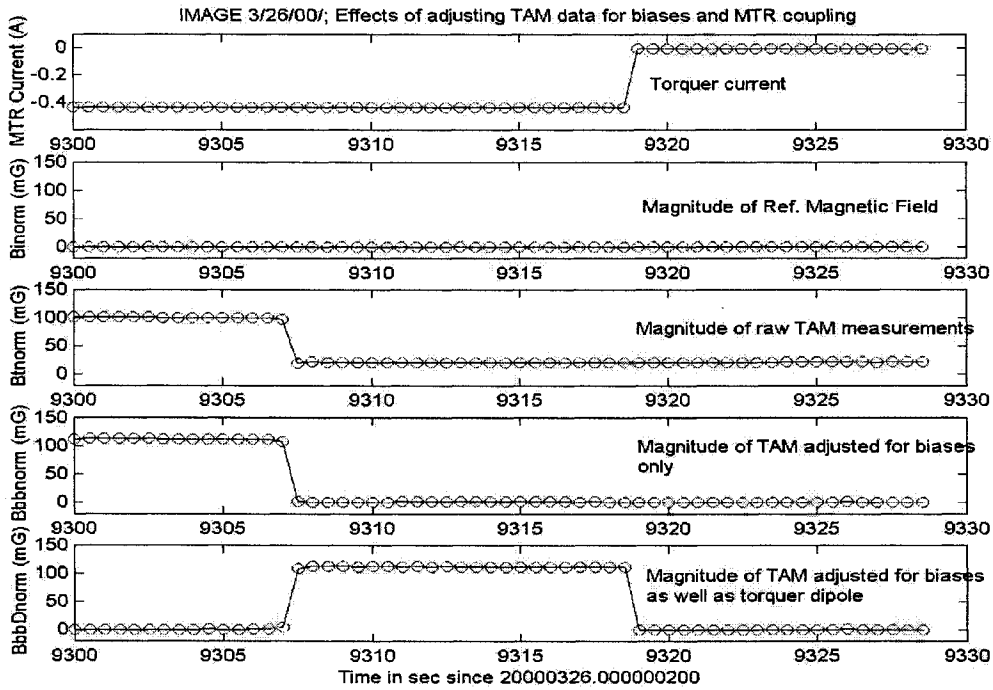


Figure 12 Discrepancies between TAM and MTR Data at Apogee of 3/26/00

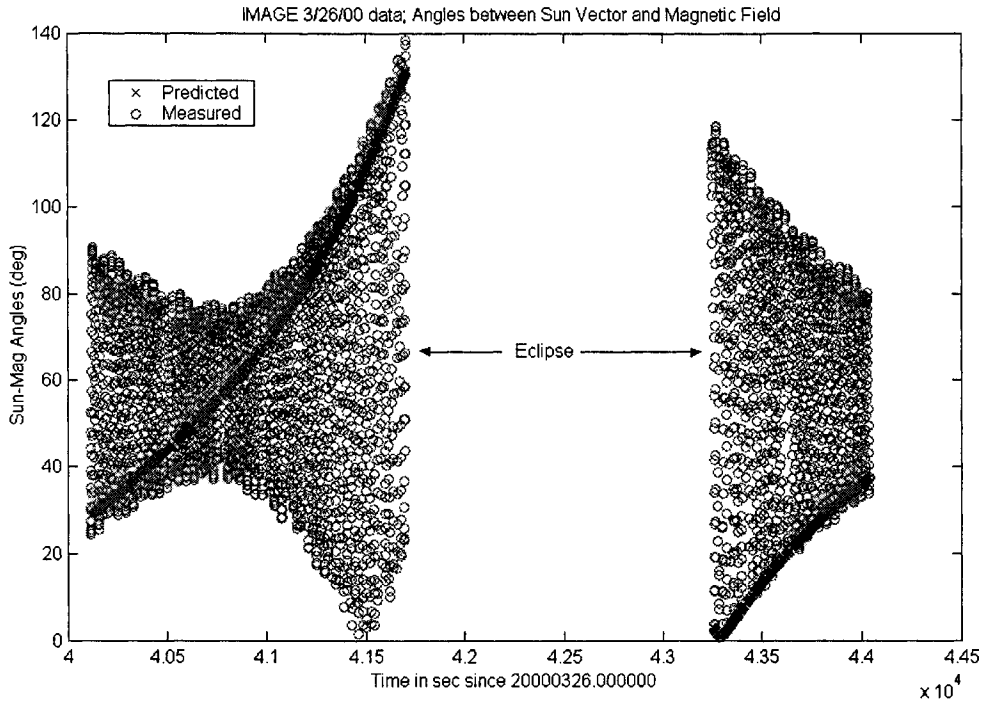


Figure 13 Sun-Mag Angles in BCS and GCI frames on 3/26/00

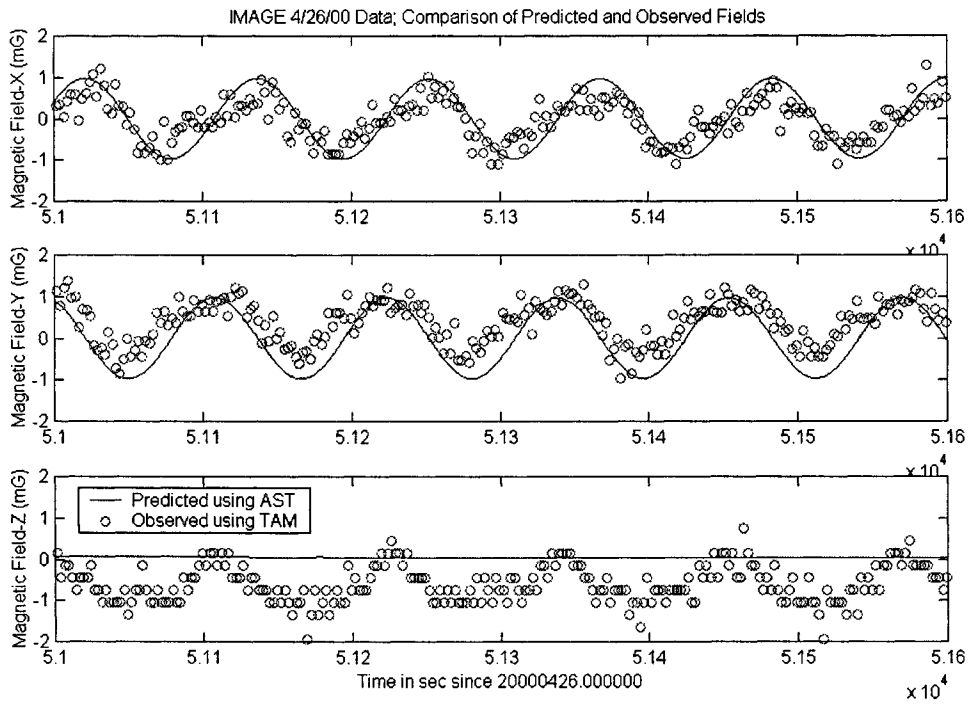


Figure 14 Comparison of Predicted and Observed Fields at Apogee on 4/26/00